Geophysical Research Letters

RESEARCH LETTER
10.1029/2020GL092223

Key Points:

- A preceding Central Pacific (CP) El Niño could generate equatorial Indian Ocean easterly anomalies leading to early thermocline shallowing
- However, ocean downwelling Kelvin waves and boreal summer equatorial westerly anomalies may arrest or reverse the initial anomalies
- Most CP El Niños do not induce a strong positive Indian Ocean Dipole, but majority of the latter is preceded by the former

Supporting Information:

- Supporting Information S1

Correspondence to
W. Cai,
Wenju.Cai@csiro.au

Citation:
Yang, K., Cai, W., Huang, G., Ng, B., & Wang, G. (2021). Is preconditioning effect on strong positive Indian Ocean Dipole by a preceding Central Pacific El Niño deterministic? *Geophysical Research Letters*, *48*, e2020GL092223. https://doi.org/10.1029/2020GL092223

Received 19 DEC 2020
Accepted 14 FEB 2021

Is Preconditioning Effect On Strong Positive Indian Ocean Dipole by a Preceding Central Pacific El Niño Deterministic?

Kai Yang[1,2,3], Wenju Cai[3,4], Gang Huang[1], Benjamin Ng[3], and Guojian Wang[3,4]

[1]State Key Laboratory of Numerical Modeling for Atmospheric Sciences and Geophysical Fluid Dynamics, Institute of Atmospheric Physics, Chinese Academy of Sciences, Beijing, China, [2]Key Laboratory of Meteorological Disaster(KLME), Ministry of Education & Collaborative Innovation Center on Forecast and Evaluation of Meteorological Disasters(CIC-FEMD), Nanjing University of Information Science & Technology, Nanjing, China, [3]Center for Southern Hemisphere Oceans Research (CSHOR), CSIRO Oceans and Atmosphere, Hobart, TAS, Australia, [4]Frontier Science Centre for Deep Ocean Multispheres and Earth System and Physical Oceanography Laboratory, Ocean University of China, China and Qingdao National Laboratory for Marine Science and Technology, Qingdao, China

Abstract The 2018 Central Pacific (CP) El Niño preceded the 2019 strong positive Indian Ocean Dipole (pIOD). The robustness of a CP El Niño preconditioning a strong pIOD has not been investigated. Here, we show that March-April-May (MAM) easterly anomalies over the equatorial eastern Indian Ocean (EIO) induced by a preceding CP El Niño drive a thermocline shallowing conducive to an early equatorial EIO cooling. However, the same winds also generate off-equatorial downwelling Rossby waves in the southern EIO, which reflect as downwelling Kelvin waves, able to weaken the initial anomalies. Furthermore, zonal winds in June-July-August (JJA) can either be beneficial or unfavorable for the developing pIOD. Only when the equatorial easterlies, EIO cooling, and thermocline shallowing are sufficiently amplified by JJA does a strong pIOD occur. Despite this, a multi-century model simulation suggests that development of majority of strong pIOD events is facilitated by a preceding CP El Niño.

Plain Language Summary The strong pIOD event in 2019, featuring strong cooling in the east and mild warming in the west Indian Ocean, induced devastating climate extremes over the populous Indian Ocean-rim countries. Its impact was amplified by the preceding CP El Niño, which has been suggested to play an important role in the generation of the 2019 strong pIOD. This study investigated the relationship of a strong pIOD with a preceding CP El Niño based on observations and model outputs. The results show that a CP El Niño in the preceding December-January-February and MAM has a preconditioning effect for development of a following strong pIOD in JJA, by generating easterly anomalies and shoaling the thermocline over the equatorial EIO in late May. However, the easterly anomalies also generate off-equatorial downwelling Rossby waves which reflect at the western boundary as downwelling Kelvin waves. The downwelling Kelvin waves may weaken the preconditioning effect, or even trigger negative IODs. In addition, JJA stochastic westerlies are detrimental to initial EIO cooling. Thus, whether a preceding CP El Niño leads to a strong pIOD is not deterministic, and is to some extent random, although strong pIOD appears to be more likely when preconditioned by a CP El Niño.

1. Introduction

A positive Indian Ocean Dipole (pIOD) develops in June-July-August (JJA) and peaks in September-October-November (SON), when the seasonal thermocline in the southeastern Indian Ocean is shallow (Saji et al., 1999; Webster et al., 1999). The associated cool sea surface temperature (SST) anomalies in the equatorial eastern Indian Ocean (EIO) and warm SST anomalies in the equatorial western Indian Ocean influence climate extremes in surrounding countries (Abram et al., 2003; Behera et al., 2005; Hashizume et al., 2012; Ummenhofer et al., 2009). Growth of initial cold SST anomalies off Sumatra-Java is dominated by Bjerknes-like positive feedback, in which the cold SST anomalies, anomalous southeasterlies, shallowing thermocline and upwelling off the Sumatra-Java coast reinforce each other (Saji et al., 1999; Webster et al., 1999). The resulting dipole pattern is usually described by a dipole mode index (DMI), defined as a zonal temperature

gradient between the western (50°E–70°E, 10°S–10°N) and eastern (90°E–110°E, 10°S–0°S) equatorial Indian Ocean (Saji et al., 1999).

During strong pIOD events, as in 1994, 1997, 2006, and 2019, the cooling off Sumatra-Java extended northward toward the Equator and then westward along the Equator, shifting atmospheric convection to the far west (Cai et al., 2020). The massive atmospheric re-organization induced devastating floods, landslides, and malaria outbreaks in the eastern African countries, and catastrophic droughts and bushfires over Indonesia and southeast Australia (Ashok et al., 2003; Behera et al., 2005; Black et al., 2003; Cai et al., 2009; Hashizume et al., 2012; Ummenhofer et al., 2009; Wang & Cai, 2020).

The impact of the 2019 strong pIOD was particularly devastating. For Australia, the 2019/2020 bushfire season, referred to as the "Black Summer," commenced early and was uncharacteristically extensive in affected area. Fires broke out in June 2019 in northeastern Australia, followed by forests burning out of control between September 2019 and March 2020 (Cai et al., 2020; Wang et al., 2020b). By early March 2020, an area of 180,000 square kilometers was burnt, at least 34 people killed, one billion animals perished, and 59,000 buildings, including 3000 homes destroyed (Cai et al., 2020; Richards et al., 2020). In east Africa, the 2019 short rain season (October-December) was one of the wettest in recent decades, after a wet short rain season in 2018. Massive floods and destructive landslides occurred across the region, with estimates of over 2.8 million people adversely affected (Wainwright et al., 2020).

Climate variability of the Indian and Pacific Oceans are related, especially the IOD and ENSO (Abram et al., 2020; Cai et al., 2019; Fan et al., 2017; Le & Bae, 2019; Le et al., 2020; Nagura & Konda, 2007; Stuecker et al., 2017; Wang & Wang, 2014; Zhao et al., 2019). However, previous research about the connection between the IOD and ENSO has mainly focused on their concurrent coupling. The dynamics of the 2019 strong pIOD are suggested to be closely related to the preceding CP warming condition in 2018 (Doi et al., 2020). Propagation of oceanic downwelling Rossby waves due to equatorial easterly anomalies of early 2019 and its reflection at the western boundary contribute to an equatorial zonal SST gradient and trigger pIOD development (Du et al., 2020). The prolonged massive impact of the 2019 strong pIOD was also related to the 2018 CP El Niño condition, which is more conducive to dry conditions over eastern Australia than eastern Pacific (EP) El Niño (Wang & Cai, 2020). The strong pIOD event in 1994 had similar features to those of the 2019 strong pIOD (Doi et al., 2020) and was also preceded by a CP El Niño condition.

Contrasting the suggested connection between the 2019 strong pIOD and the 2018 El Niño condition is an suggestion that an El Niño, especially a strong El Niño, may limit the development of pIOD in the year after by generating off-equatorial downwelling Rossby waves in the southern EIO; the Rossby waves reflect at the western boundary as eastward propagating downwelling Kelvin waves, which deepen the thermocline in the EIO and may even result in a negative IOD (Chen et al., 2019; Du et al., 2020; Xie et al., 2002). As such, how an El Niño influences development of an IOD event has not been fully investigated.

In this study, we have examined the relationship between pIOD, specifically the strong pIOD and its preceding El Niño condition based on observations and model outputs. Considering the different relationship between CP El Niño or EP El Niño and the IOD (Zhang et al., 2015), here we focused on the relationship of preceding CP El Niño with pIOD events.

2. Data and Methods

2.1. Observations

We use SST (potential temperature at 5 m depth), potential temperature, and wind stress (momentum flux) from the NCEP Global Ocean Data Assimilation System (GODAS) dataset for the period of 1980–2019, with a 0.333° latitude and 1.0° longitude grid (Behringer & Xue, 2004). The anomalies of each variable are calculated referenced to the climatology of the full period, and quadratically detrended.

2.2. Depiction of Observed pIOD and ENSO Diversity

As is described in previous studies, dynamics of strong pIOD are different from that of moderate pIOD (Cai et al., 2014, 2020). During a strong pIOD, initial cold anomalies off Sumatra-Java extend toward the

Equator, and the equatorial easterly anomalies strengthen, triggering equatorial nonlinear zonal, and nonlinear vertical oceanic advection, favoring fast growth of the equatorial surface cooling (Cai et al., 2014). A separate index for strong pIOD events is constructed based on the normalized first two principal components (PC1 and PC2) from Empirical Orthogonal Function (EOF) analysis of observed SON SST anomalies over the tropical Indian Ocean (5°S–5°N and 40°E–100°E). The two PCs have a nonlinear relationship (Cai et al., 2020; Yang et al., 2020), that is, $PC2(t) = \alpha[\mathrm{PC1}(t)]^2 + \beta\mathrm{PC1}(t) + \gamma$. EOF1 features an all-event average pattern, analogous to that associated with the DMI, showing the dipole SST structure with a shoaled equatorial thermocline in the east but a deepened thermocline to the west. EOF2 displays an equatorially north-south symmetric cooling maximum in the east and at subsurface, reflecting the effect of equatorial nonlinear oceanic advection (Yang et al., 2020). During a strong pIOD, the equatorially symmetric cold anomalies of the EOF2 pattern superimposes onto the cold anomalies off Sumatra-Java of EOF1, such that it features strong westward-extended cold anomalies along the equator (Cai et al., 2020). A strong pIOD is defined as S-index = (PC1+PC2)/$\sqrt{2}$ larger than 1.5 standard deviation (s.d.). Following Cai et al. (2014), a moderate pIOD is described as when DMI > 0.5 s.d. and S-index < 1.5 s.d. (a pIOD but not a strong event), and a negative IOD (nIOD) is described as when DMI < −0.5 s.d.

CP and EP ENSO have been separated using a similar EOF analysis over the tropical Pacific (15°S–15°N and 140°E–80°W) based on monthly SST data. CP and EP ENSO are represented by C-index = ($\mathrm{PC1_{ENSO}}$ + $\mathrm{PC2_{ENSO}}$)/$\sqrt{2}$ and E-index = ($\mathrm{PC1_{ENSO}}$-$\mathrm{PC2_{ENSO}}$)/$\sqrt{2}$, respectively (Cai et al., 2018; Karamperidou et al., 2017; Takahashi et al., 2011; Wang et al., 2020a). A CP El Niño event is identified as C-index > 0.5 s.d.

2.3. Model Outputs

Considering the limited events in observations, a 1,801 years long preindustrial, fully coupled control simulation from Community Earth System Model (CESM-control; Kay et al., 2015) is used to confirm the relationships and mechanisms in observations. The same approach is applied to the CESM-control to calculate the anomalies of each variable as in observations.

The CESM-control shows a reasonable ability in simulating the nonlinearity of the first two PCs of EOF over the tropical Indian Ocean and the Pacific Ocean (Figure S1). The strong and moderate pIOD, and the EP and CP ENSO are well separated in this model. The nonlinear coefficients (|α|) of the PCs are 0.88 and 0.29 for the Indian Ocean and Pacific Ocean, respectively. These are comparable to that in observations, which is 0.45 for the IOD (Yang et al., 2020) and 0.31 for ENSO (Cai et al., 2018), respectively. Cai et al. (2020) suggests that the two regions defined by the DMI may not be suitable for describing the IOD in models. In the CESM-control, we use the PC1 of EOF instead of the DMI to define the IOD events. The definition of strong pIOD and CP El Niño is similar to that in observations, while the moderate pIOD is described as when S-index < 1.5 s.d., and PC1 > 1 s.d.; nIOD is defined as when the PC1 < 0.

3. Results

3.1. Impact From a Preceding CP El Niño on Strong pIOD

Since 1980, there are four strong pIOD events defined as when the S-index > 1.5 s.d. (1994, 1997, 2006, and 2019), among which two events (1994 and 2019) are preceded by a CP El Niño condition in the previous D(-1)JF ("D(-1)" indicates previous December) and MAM season (Figures 1a and 1b). Here we examine the CP El Niño condition in D(-1)JF and MAM because oceanic Rossby waves associated with the CP El Niño condition of the two seasons may influence the tropical Indian Ocean subsurface temperatures in the subsequent seasons (Du et al., 2020). In 1997, the early development of the extraordinary EP El Niño generates conducive easterly wind anomalies and contributes to the development of the strong pIOD (Yang et al., 2015). Below we compare the development of strong pIOD in 2006, 1994, and 2019 to elucidate the preconditioning effect of a preceding CP El Niño.

The evolution of SST and wind stress anomalies in the 1994 and 2019 strong pIOD are similar (Doi et al., 2020), and are both accompanied by preceding CP El Niños from D(-1)JF to SON (Figure 1c). The easterly anomalies associated with the preceding CP El Niño condition are seen over the EIO in MAM,

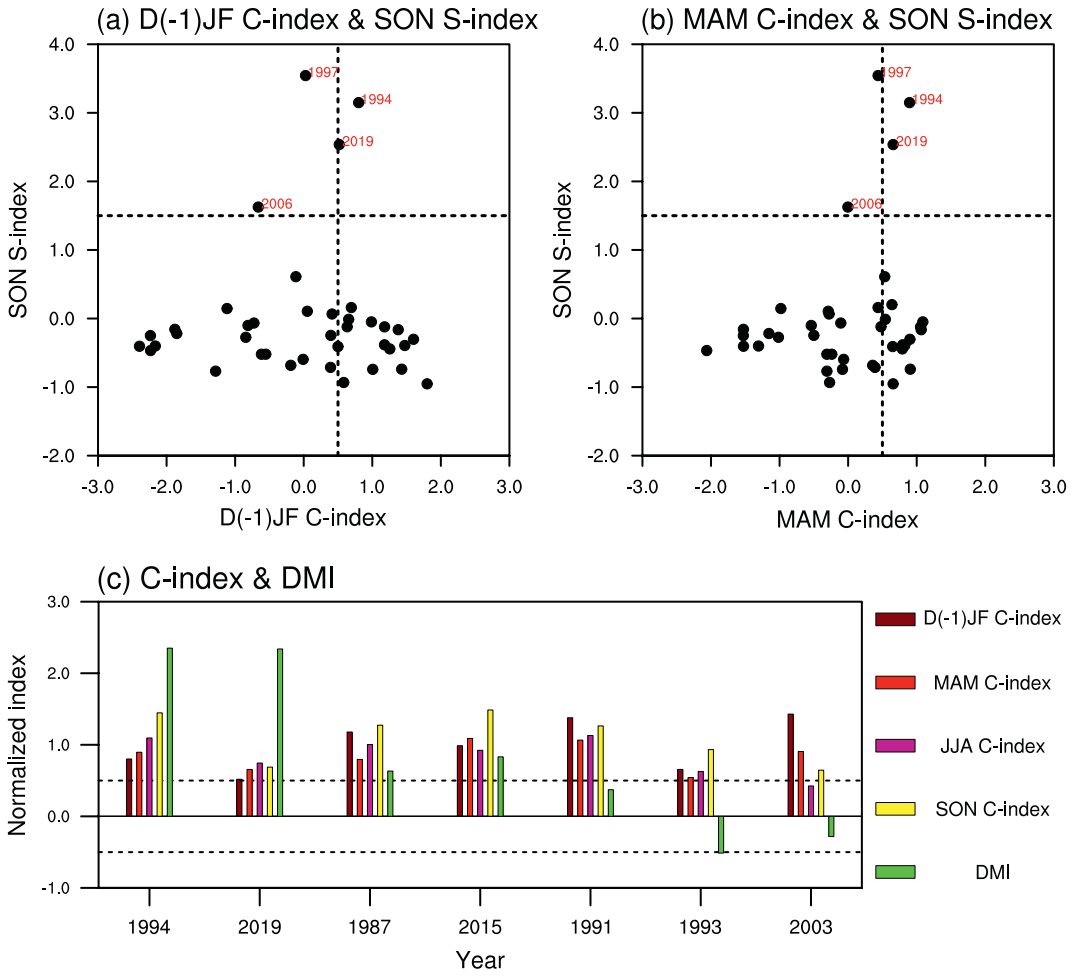

Figure 1. The relationship of a preceding Central Pacific (CP) El Niño and a pIOD in observations. (a and b) Relationship of (a) D(-1)JF C-index and (b) March-April-May (MAM) C-index with September-October-November (SON) S-index in the Global Ocean Data Assimilation System (GODAS) dataset for the period of 1980–2019. A CP El Niño is defined as C-index > 0.5 s.d. A strong pIOD is described as S-index >1.5 s.d. There are four strong positive Indian Ocean Dipole (pIOD) events in the past 40 years, shown in red. The horizontal and vertical dashed lines show the 1.5 s.d. for S-index and 0.5 s.d. for C-index, respectively. (c) Normalized D(-1)JF, MAM, June-July-August (JJA), SON C-index, and SON DMI of all 7 years with D(-1)JF, MAM, SON C-index > 0.5 s.d. Events of pIOD and nIOD are defined as DMI>0.5 s.d. and DMI < −0.5 s.d., respectively. The dashed lines show the 0.5 s.d. of the C-index and DMI.

which contribute to a shallower thermocline in the equatorial EIO compared to the absence of a preceding CP El Niño in 2006 (Figures 2a and 2d). The shoaled thermocline by late May when the seasonal easterlies start to establish over the equatorial EIO, provides a favorable condition for the development of a pIOD.

In the meantime, the easterly anomalies generate off-equatorial downwelling Rossby waves in the southern EIO, which propagate westward and warm the west tropical Indian Ocean. The MAM heat content anomalies in the tropical western Indian Ocean (20°S–20°N, and 40°E–80°E) are significantly correlated with the MAM C-index (with a correlation coefficient of 0.51, significant above the 99% confidence level). This contributes to a west-minus-east SST gradient that in turn favors development of enhanced easterly wind anomalies (Du et al., 2020), particularly when cool anomalies have been amplified by the local Bjerknes feedback, aided for example by a concurrent El Niño. The shallow thermocline and easterly anomalies result in pIOD development in JJA and eventually into a stronger pIOD in the mature season (SON) in 1994 and 2019 than that in 2006 (Figure 2).

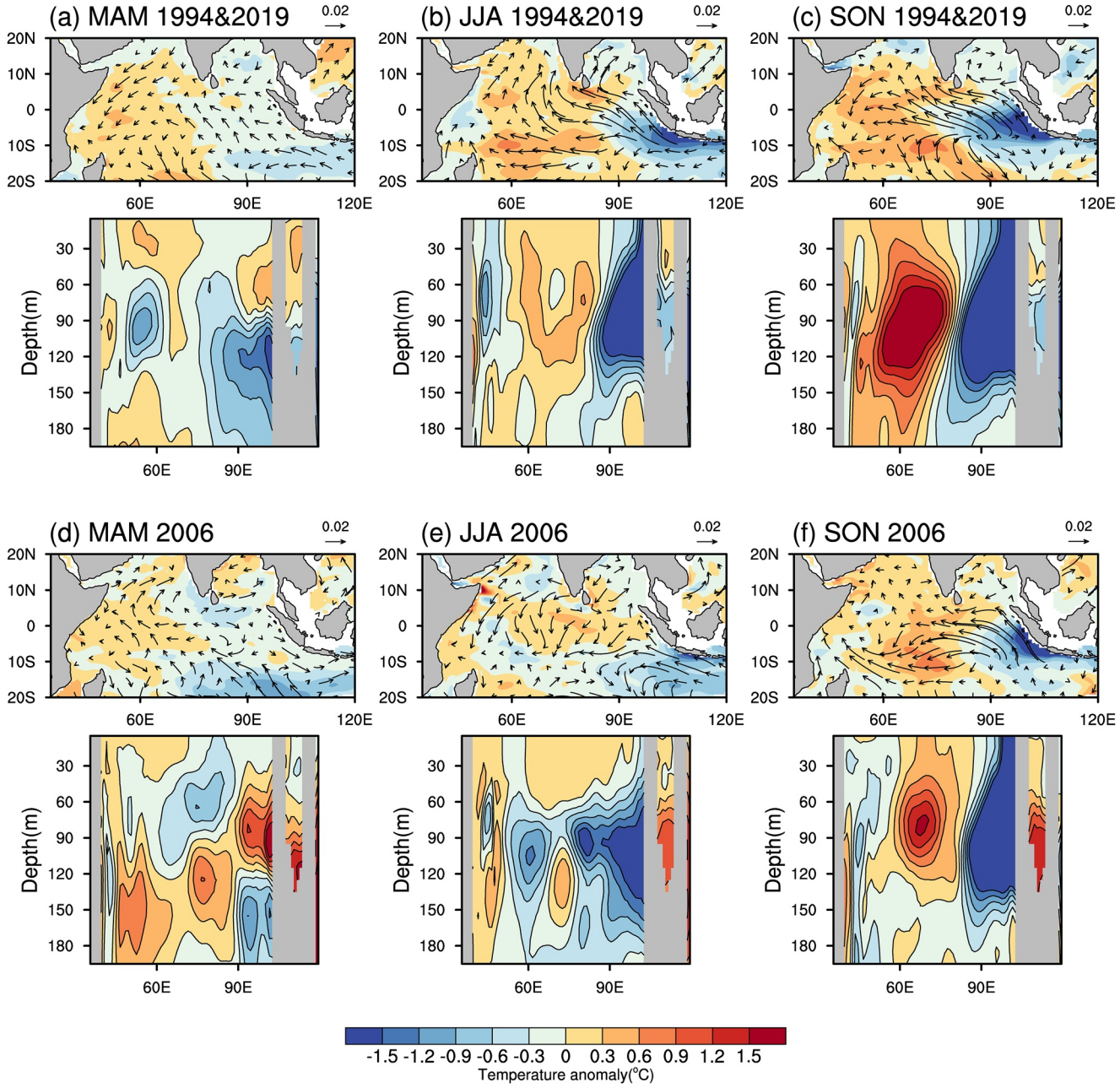

Figure 2. Comparison between strong pIOD preceded and not preceded by a CP El Niño in observations. (a–c) The SST (°C, color, and upper panel), wind stress (N m^{-2}, vectors, and upper panel) and vertical potential temperature (°C, and lower panel) anomalies in (a) MAM, (b) JJA, and (c) SON averaged over 1994 and 2019 in the GODAS data. The vertical potential temperature is calculated as the average over 5°S–5°N (d–f) Same as in (a–c), but for 2006.

3.2. Nondeterministic Outcome of a Preceding CP El Niño

However, a CP El Niño in D(-1)JF and MAM does not always result in a strong pIOD in SON, even with enforcement of a concurrent El Niño, which provides pIOD-favoring equatorial easterly anomalies (Figure S2). Besides 1994 and 2019, there are another five years with C-index > 0.5 s.d. in D(-1)JF, MAM, and SON. Among them, in 1987 and 2015 when a moderate pIOD developed and in the other 3 years (1991, 1993, and 2003), neutral or a nIOD followed (Figure 1c). As discussed earlier, the same easterly anomalies generate off-equatorial downwelling Rossby waves in the southern EIO. These Rossby waves reflect at the western boundary as downwelling Kelvin waves and halt the shoaling of the EIO thermocline (Chen et al., 2019; Du et al., 2020). In addition, equatorial wind variability over the Indian Ocean is strong in JJA, influenced

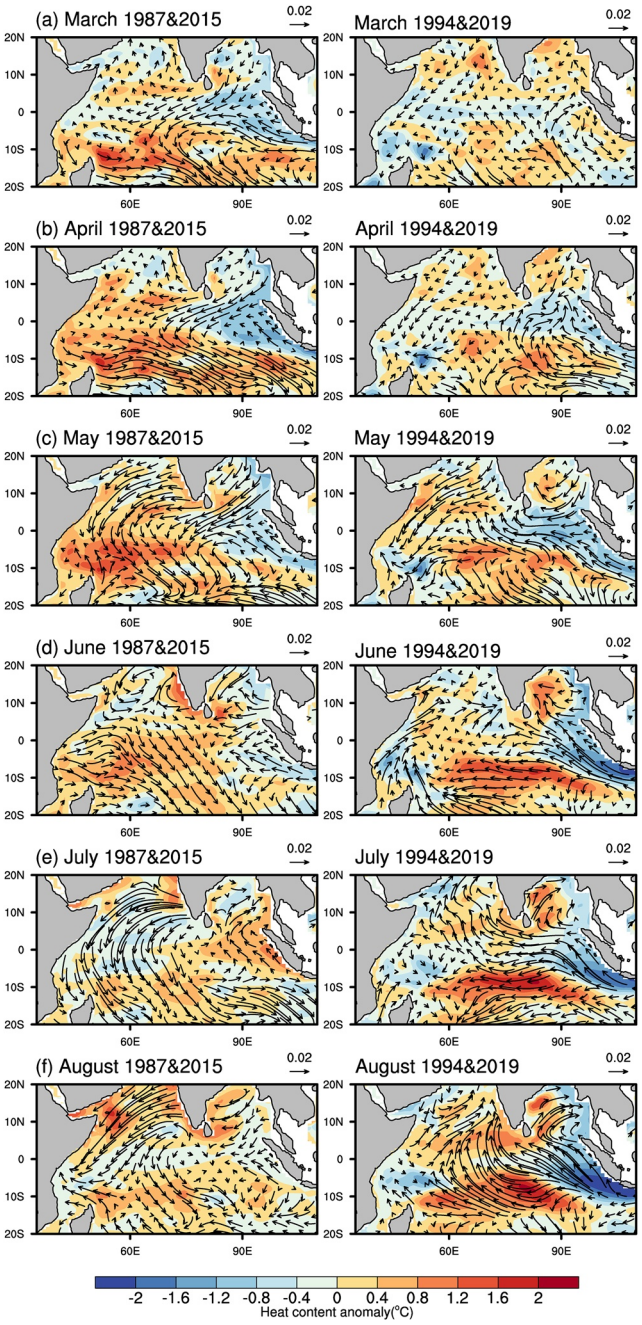

Figure 3. Evolution of moderate and strong pIOD preceded by a CP El Niño in observations. (a) Upper ocean heat content calculated as averaged potential temperature over the upper 200 m (°C, color) and wind stress (N m^{-2}, vectors) anomalies in March. The left panel shows the anomalies averaged over 1987 and 2015, the right panel shows the anomalies averaged over 1994 and 2019 (b–f) Same as in (a), but for (b) April, (c) May, (d) June, (e) July, and (f) August, respectively.

by a number of factors, such as the Indian summer monsoon, Australian high, and Northwestern Pacific Subtropical High (Abram et al., 2007; Lu & Ren, 2020; Sun et al., 2015; Yang et al., 2015). Anomalous westerlies are unfavorable for development of a pIOD event.

Focusing on 1987 and 2015, the equatorial easterly anomalies and the associated shoaled thermocline are seen in March accompanied by downwelling Rossby waves in the southern tropical Indian Ocean (Figure 3a, left panel), which reflect at the western boundary in April (Figure 3b, left panel). The reflected downwelling Kelvin waves, together with the downwelling Kelvin waves associated with the equatorial westerly anomalies over the western tropical Indian Ocean, arrest the shallowing of the EIO thermocline by June and July (Figures 3c–3e, left panel). The moderate pIOD restarts from August (Figure 3f, left panel).

Only when the equatorial easterlies, EIO cooling, and thermocline shallowing are sufficiently amplified by JJA does a strong pIOD occurs, as in 1994 and 2019. In these two years, although the equatorial easterly anomalies and the associated shoaled thermocline develop later (in April) than that in 1987 and 2015 (Figures 3a and 3b, right panel), the timing is optimal such that the initial cool anomalies are able to be amplified from May to August (Figures 3c–3f, right panel). The downwelling Kelvin waves reflect in May and June, a time when Bjerknes feedback starts to operate. The easterly anomalies and shoaled thermocline in the EIO persist, leading to substantial cool anomalies (Figures 3c and 3d, right panel). These pIOD anomalies are able to outweigh the impact of the reflected downwelling Kelvin waves. The thermocline remains shallow into July and shoals further in August (Figures 3e and 3f, right panel), and the associated wind and SST anomalies grow into a strong pIOD in SON. In addition, other difference between the two groups of events, such as warmer SST over north Indian Ocean in 1994 and 2019 than that in 1987 and 2015, may also contribute to the difference of zonal wind anomalies over the tropical Indian Ocean and the associated development of pIOD (Figures 3e and 3f).

3.3. The Role of Boreal Summer Equatorial Wind Variability

That a preceding CP El Niño may not always lead to equatorial Indian Ocean easterly anomalies in JJA (Figure S2) is key to understanding the nondeterministic outcome. Stochastic westerlies not only can cancel the preconditioning effect of a CP El Niño but also can reverse the associated initial cooling. For example, in 1991, the western tropical Indian Ocean shows enormous westerly anomalies by May and June, as the downwelling Kelvin waves are more than enough to wipe out the initial EIO shoaled thermocline anomalies and generate a deepened EIO thermocline as seen in June (Figure S3, left panel); the reinvigorated EIO cool anomalies are ultimately small (Figure 1c). In 1993, the easterly anomalies and any associated shoaled EIO thermocline anomalies are hardly established by MAM, and the EIO shows westerly anomalies in JJA, producing a negative IOD (Figure S3, middle panel). In 2003, the shoaled thermocline over the EIO in April is reduced by the westerly anomalies in May, and a premature pIOD develops in June and vanishes in August (Figure S3, right panel).

Thus, whether the preceding CP El Niño leads to a specific outcome is to a degree random, depending on not only the shallowing directly from the associated easterly anomalies, the relative strength of the EIO thermocline deepening associated with the reflection, timing of the reflection, but also stochastic wind forc-

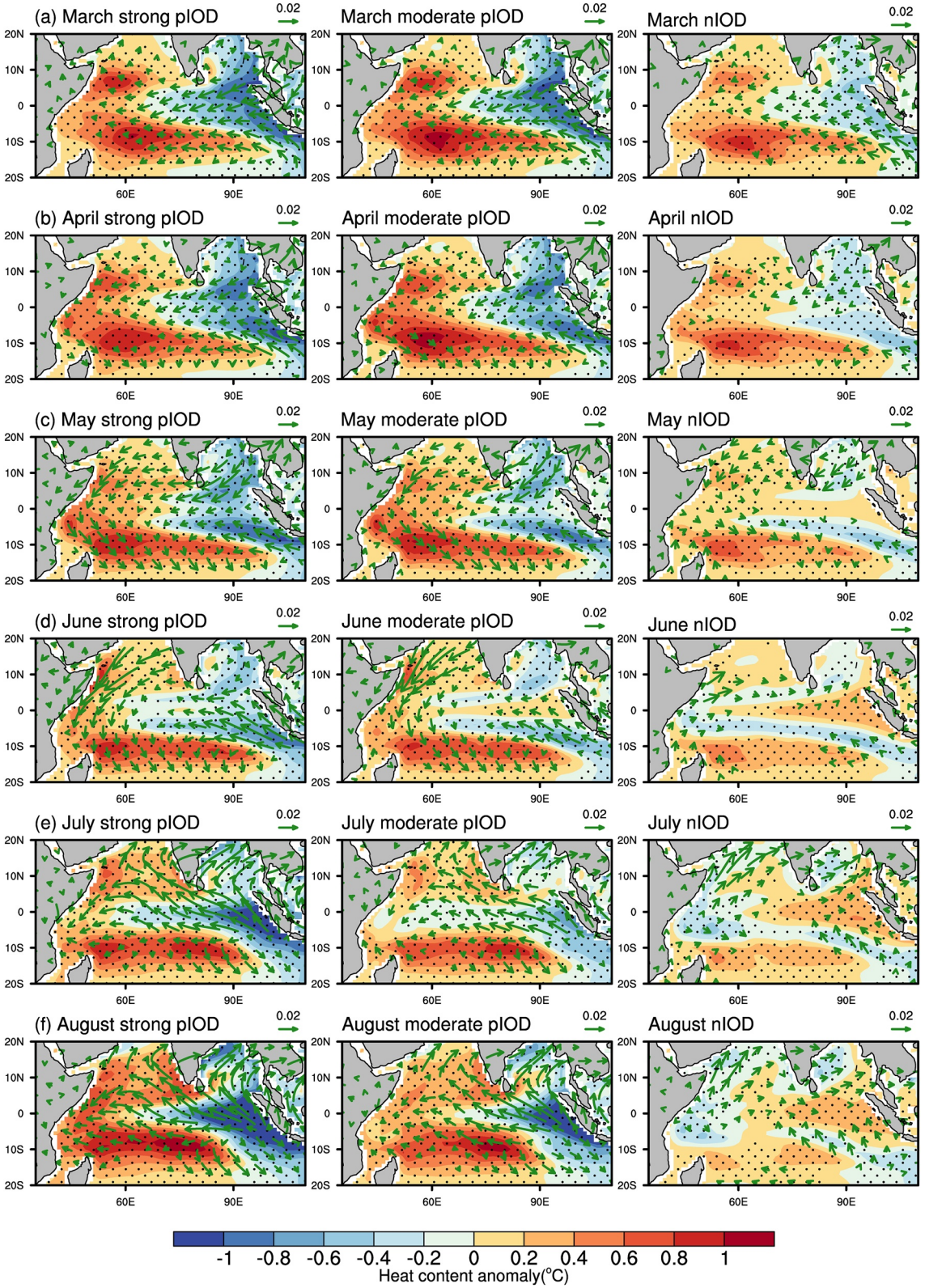
(a) March strong pIOD
March moderate pIOD
March nIOD
(b) April strong pIOD
April moderate pIOD
April nIOD
(c) May strong pIOD
May moderate pIOD
May nIOD
(d) June strong pIOD
June moderate pIOD
June nIOD
(e) July strong pIOD
July moderate pIOD
July nIOD
(f) August strong pIOD
August moderate pIOD
August nIOD
0.02
20N
10N
0
10S
20S
60E
90E
-1 -0.8 -0.6 -0.4 -0.2 0 0.2 0.4 0.6 0.8 1
Heat content anomaly(°C)

ing. For example, if the reflection occurs after the seasonal Bjerknes feedback substantially amplifying the initial cool anomalies and thermocline shallowing, the impact of the reflection is small, as the case for the 1994/2019 strong pIOD. By contrast, in 1987 and 2015, when the impact of the reflection, and/or westerly wind forcing, is strong, a moderate pIOD is generated, as development of the pIOD is temporarily halted (Figure 3).

That equatorial easterly anomalies over the equatorial Indian Ocean in JJA are also important for a CP El Niño to induce a strong pIOD is supported by findings of previous studies. For example, easterly anomalies associated with an interhemispheric pressure gradient are suggested to contribute to the development of the 2019 strong pIOD (Lu & Ren, 2020). On the contrary, westerly anomalies over EIO may arrest the preconditioning effect of a CP El Niño and result in a neutral or even a nIOD condition (Figure S3). Thus, high variability of equatorial Indian Ocean zonal wind in JJA, which has been suggested to be related to internal variability of the Indian Ocean, Indian summer monsoon, Australian high, and Northwestern Pacific Subtropical High (Lu & Ren, 2020; Sun et al., 2015; Yang et al., 2015), appears to contribute to the nondeterministic preconditioning on strong pIOD by a preceding CP El Niño.

3.4. Mechanisms Confirmed by Model Simulation

The robustness of a CP El Niño preconditioning a strong pIOD is limited by the rare strong pIOD events in observations. Examination of the long simulation of CESM-control finds that 79% of the strong pIOD are preceded by a CP El Niño condition in MAM. This confirms that the preconditioning effect of the CP El Niño plays an important role in the development of strong pIOD (Figure S4). However, majority of CP El Niño are not followed by a strong pIOD.

However, the result from the CESM-control also supports a lack of deterministic effects of a preceding CP El Niño on a strong pIOD. Similar to observations, a CP El Niño in both D(-1)JF and MAM may either be followed by a strong pIOD, moderate pIOD, or a nIOD event, even though all with a concurrent CP El Niño condition in SON that favors development of a pIOD (Figure 4). For cases in which a strong pIOD eventuates in SON, the preceding CP El Niño shoals the equatorial EIO thermocline and generates off-equatorial downwelling Rossby waves over the southwestern tropical Indian Ocean in MAM (Figures 4a–4c, left panel). The shoaled equatorial EIO thermocline and the east-west temperature gradient in May favor easterly anomalies and the establishment of positive Bjerknes feedback in JJA, facilitating a strong pIOD (Figure 4e and 4f, left panel).

Compared with strong pIOD cases, in years when a CP El Niño condition in D(-1)JF and MAM leads to a moderate pIOD in SON, there are similar thermocline (or heat content) and easterly wind anomalies in March. However, a stronger effect of downwelling Rossby waves is seen in April (Figures 4a–4c, middle panel). The weaker shallowing of the equatorial EIO thermocline is completely wiped out by the reflected downwelling Kelvin waves by June, in spite of easterly anomalies over the EIO (Figure 4d, middle panel). Development of the moderate pIOD restarts in July (Figure 4e and 4f, middle panel).

When the easterly anomalies associated with the preceding CP El Niño are weak in MAM (Figure S5), the shoaling of the thermocline is small. The weak thermocline and cool anomalies can be easily arrested by the reflected downwelling Kelvin waves, which may even lead to a deepened thermocline in the EIO by JJA, and eventually to a nIOD (Figures 4a–4f, right panel).

In addition, the JJA C-index during pIOD (strong or moderate) events is smaller than the C-index in nIOD events, while the JJA E-index during pIOD events is generally larger than the E-index in the nIOD events, which might suggest that some pIODs are coupled with EP El Niño in JJA in addition to preconditioning associated with a positive C-index (Figure S5), as in 1997.

Figure 4. Preconditional effect on IOD events by a preceding CP El Niño in CESM-control. (a) Composite of the heat content (ºC, color) and wind stress (N m^{-2}, vectors) anomalies in March for years with D(-1)JF, MAM, and SON C-index > 0.5, and eventually develop to a strong pIOD (left panel, 86 events, S-index > 1.5 s.d.), a moderate pIOD (middle panel, 94 events, S-index < 1.5 s.d. and PC1 > 1.0 s.d.), and a negative pIOD (right panel, 69 events, PC1 < 0) in SON. Black stippling shows areas where the heat content anomalies are significant above the 95% confidence level. For the wind anomalies, only those significant above the 95% confidence level are shown. The heat content is calculated as the average potential temperature over the upper 200 m (b–f) Same as in (a), but for (b) April, (c) May, (d) June, (e) July, and (f) August, respectively.

4. Conclusions

A CP El Niño condition in D(-1)JF and MAM favors easterly anomalies and a shallowed thermocline over the equatorial EIO. These may provide a beneficial precondition for early development of a strong pIOD and "seed anomalies" for the positive Bjerknes feedback, which starts to operate in late May. However, a CP El Niño is not always followed by a strong or a moderate pIOD. This is partly due to the fact that the same easterly anomalies also generate off-equatorial downwelling Rossby waves which reflect at the western boundary as equatorial downwelling Kelvin waves, potentially halting or even reversing the shoaling of the equatorial EIO thermocline anomalies. Another offsetting factor is equatorial winds in JJA which have a high variability. Easterly anomalies over the equatorial Indian Ocean in JJA can reinforce the shoaled thermocline associated with the preceding CP El Niño and lead to a strong pIOD, whereas the westerly anomalies can arrest the preconditioning effect and lead to a neutral or even a nIOD condition. These results have been confirmed by a multi-century preindustrial control simulation from CESM, in which 79% of the strong pIOD events are preceded by a CP El Niño in MAM, suggesting that a strong pIOD is more likely to occur when preceded by a preceding CP El Niño.

Data Availability Statement

The data used in this study can be downloaded from the websites below:

GODAS: https://psl.noaa.gov/data/gridded/data.godas.html;

CESM-control: https://www.earthsystemgrid.org/dataset/ucar.cgd.ccsm4.CESM_CAM5_BGC_LE.html?df=true.

Acknowledgments
This work is supported by the Strategic Priority Research Program of Chinese Academy of Sciences, Grant No. XDB40000000. Gang Huang is supported by the National Natural Science Foundation of China (91937302, 41831175), the Strategic Priority Research Program of Chinese Academy of Sciences (XDA20060501). Kai Yang is supported by China Postdoctoral Science Foundation (2018M640168), Open Research Fund Program of Key Laboratory of Meteorological Disaster of Ministry of Education (Nanjing University of Information Science and Technology) Grant No. KLME201806 and a scholarship from China Scholarship Council. Wenju Cai, Guojian Wang, and Benjamin Ng are supported by CSHOR, a joint research Center for Southern Hemisphere Oceans Research between QNLM and CSIRO; Wenju Cai and Guojian Wang are also supported by the Earth Systems and Climate Change Hub of the Australian Government's National Environmental Science Program.

References

Abram, N. J., Gagan, M. K., Liu, Z., Hantoro, W. S., McCulloch, M. T., & Suwargadi, B. W. (2007). Seasonal characteristics of the Indian Ocean Dipole during the Holocene epoch. *Nature*, *445*(7125), 299–302. https://doi.org/10.1038/nature05477

Abram, N. J., Gagan, M. K., McCulloch, M. T., Chappell, J., & Hantoro, W. S. (2003). Coral Reef Death during the 1997 Indian Ocean Dipole linked to Indonesian wildfires. *Science*, *301*(5635), 952–955. www.jstor.org/stable/3834840

Abram, N. J., Wright, N. M., Ellis, B., Dixon, B. C., Wurtzel, J. B., England, M. H., et al. (2020). Coupling of Indo-Pacific climate variability over the last millennium. *Nature*, *579*(7799), 385–392. https://doi.org/10.1038/s41586-020-2084-4

Ashok, K., Guan, Z., & Yamagata, T. (2003). Influence of the Indian Ocean Dipole on the Australian winter rainfall. *Geophysical Research Letters*, *30*(15), 1821. https://doi.org/10.1029/2003GL017926

Behera, S. K., Luo, J.J., Masson, S., Delecluse, P., Gualdi, S., Navarra, A., & Yamagata, T. (2005). Paramount impact of the Indian Ocean Dipole on the East African short rains: A CGCM study. *Journal of Climate*, *18*(21), 4514–4530. https://doi.org/10.1175/JCLI3541.1

Behringer, D., & Xue, Y. (2004). Evaluation of the global ocean data assimilation system at NCEP: The Pacific Ocean. In *Paper presented at the proceedings of Eighth Symposium on Integrated Observing and Assimilation Systems for Atmosphere, Oceans, and Land Surface*.

Black, E., Slingo, J., & Sperber, K. R. (2003). An observational study of the relationship between excessively strong short rains in coastal East Africa and Indian Ocean SST. *Monthly Weather Review*, *131*(1), 74–94. https://doi.org/10.1175/1520-0493(2003)131<0074:AOSOTR>2.0.CO;2

Cai, W., Cowan, T., & Raupach, M. (2009). Positive Indian Ocean Dipole events precondition southeast Australia bushfires. *Geophysical Research Letters*, *36*(19), L19710. https://doi.org/10.1029/2009GL039902

Cai, W., Santoso, A., Wang, G., Weller, E., Wu, L., Ashok, K., et al. (2014). Increased frequency of extreme Indian Ocean Dipole events due to greenhouse warming. *Nature*, *510*(7504), 254–258. https://doi.org/10.1038/nature13327

Cai, W., Wang, G., Dewitte, B., Wu, L., Santoso, A., Takahashi, K., et al. (2018). Increased variability of eastern Pacific El Niño under greenhouse warming. *Nature*, *564*(7735), 201–206. https://doi.org/10.1038/s41586-018-0776-9

Cai, W., Wu, L., Lengaigne, M., Li, T., McGregor, S., Kug, J.-S., et al. (2019). Pantropical climate interactions. *Science*, *363*(6430), eaav4236. https://science.sciencemag.org/content/sci/363/6430/eaav4236.full.pdf

Cai, W., Yang, K., Wu, L., Huang, G., Santoso, A., Ng, B., et al. (2020). Opposite response of strong and moderate positive Indian Ocean Dipole to global warming. *Nature Climate Change*, *11*, 27–32. https://doi.org/10.1038/s41558-020-00943-1

Chen, Z., Du, Y., Wen, Z., Wu, R., & Xie, S.-P. (2019). Evolution of south tropical Indian Ocean warming and the climatic impacts following strong El Niño events. *Journal of Climate*, *32*(21), 7329–7347. https://doi.org/10.1175/JCLI-D-18-0704.1

Doi, T., Behera, S. K., & Yamagata, T. (2020). Predictability of the super IOD event in 2019 and its link with El Niño Modoki. *Geophysical Research Letters*, *47*(7), e2019GL086713. https://agupubs.onlinelibrary.wiley.com/doi/abs/10.1029/2019GL086713

Du, Y., Zhang, Y., Zhang, L.-Y., Tozuka, T., Ng, B., & Cai, W. (2020). Thermocline warming induced extreme Indian Ocean Dipole in 2019. *Geophysical Research Letters*, *47*(18), e2020GL090079. https://doi.org/10.1029/2020GL090079

Fan, L., Liu, Q., Wang, C., & Guo, F. (2017). Indian Ocean Dipole modes associated with different types of ENSO development. *Journal of Climate*, *30*(6), 2233–2249. https://doi.org/10.1175/JCLI-D-16-0426.1

Hashizume, M., Chaves, L. F., & Minakawa, N. (2012). Indian Ocean Dipole drives malaria resurgence in East African highlands. *Scientific Reports*, *2*(1), 269. https://doi.org/10.1038/srep00269

Karamperidou, C., Jin, F.-F., & Conroy, J. L. (2017). The importance of ENSO nonlinearities in tropical pacific response to external forcing. *Climate Dynamics*, *49*(7), 2695–2704. https://doi.org/10.1007/s00382-016-3475-y

Kay, J. E., Deser, C., Phillips, A., Mai, A., Hannay, C., Strand, G., et al. (2015). The community earth system model (CESM) large ensemble project: A community resource for studying climate change in the presence of internal climate variability. *Bulletin of the American Meteorological Society*, *96*(8), 1333–1349. https://doi.org/10.1175/BAMS-D-13-00255.1

Le, T., & Bae, D.-H. (2019). Causal Links on interannual timescale between ENSO and the IOD in CMIP5 future simulations. *Geophysical Research Letters*, *46*(5), 2820–2828. https://doi.org/10.1029/2018GL081633

Le, T., Ha, K.J., Bae, D.-H., & Kim, S.-H. (2020). Causal effects of Indian Ocean Dipole on El Niño–Southern oscillation during 1950–2014 based on high-resolution models and reanalysis data. *Environmental Research Letters*, *15*(10), 1040b1046. http://dx.doi.org/10.1088/1748-9326/abb96d

Lu, B., & Ren, H.-L. (2020). What caused the extreme Indian Ocean Dipole event in 2019?. *Geophysical Research Letters*, *47*(11), e2020GL087768. https://doi.org/10.1029/2020GL087768

Nagura, M., & Konda, M. (2007). The seasonal development of an SST anomaly in the Indian Ocean and its relationship to ENSO. *Journal of Climate*, *20*(1), 38–52.

Richards, L., Brew, N., & Smith, L. (2020). *Australian bushfires—frequently asked questions: A quick guide*. (Parliament of Australia, 2020) https://www.aph.gov.au/About_Parliament/Parliamentary_Departments/Parliamentary_Library/pubs/rp/rp1920/Quick_Guides/AustralianBushfires

Saji, N. H., Goswami, B. N., Vinayachandran, P. N., & Yamagata, T. (1999). A dipole mode in the tropical Indian Ocean. *Nature*, *401*(6751), 360–363. https://doi.org/10.1038/43854

Stuecker, M. F., Timmermann, A., Jin, F.F., Chikamoto, Y., Zhang, W., Wittenberg, A. T., et al. (2017). Revisiting ENSO/Indian Ocean Dipole phase relationships. *Geophysical Research Letters*, *44*(5), 2481–2492. https://doi.org/10.1002/2016GL072308

Sun, S., Lan, J., Fang, Y., Tana, & Gao, X. (2015). A triggering mechanism for the Indian Ocean Dipoles independent of ENSO. *Journal of Climate*, *28*(13), 5063–5076. https://journals.ametsoc.org/view/journals/clim/28/13/jcli-d-14-00580.1.xml

Takahashi, K., Montecinos, A., Goubanova, K., & Dewitte, B. (2011). ENSO regimes: Reinterpreting the canonical and Modoki El Niño. *Geophysical Research Letters*, *38*, L10704. https://doi.org/10.1029/2011GL047364

Ummenhofer, C. C., England, M. H., McIntosh, P. C., Meyers, G. A., Pook, M. J., Risbey, J. S., et al. (2009). What causes southeast Australia's worst droughts?. *Geophysical Research Letters*, *36*(4). https://doi.org/10.1029/2008GL036801

Wainwright, C. M., Finney, D. L., Kilavi, M., Black, E., & Marsham, J. H. (2020). *Extreme rainfall in East Africa, October 2019–January 2020 and context under future climate change*. Weather. https://doi.org/10.1002/wea.3824

Wang, G., & Cai, W. (2020). Two-year consecutive concurrences of positive Indian Ocean Dipole and Central Pacific El Niño preconditioned the 2019/2020 Australian "black summer" bushfires. *Geoscience Letters*, *7*(1), 1–9. https://doi.org/10.1186/s40562-020-00168-2

Wang, G., Cai, W., & Santoso, A. (2020a). Stronger increase in the frequency of extreme convective than extreme warm El Nino events under greenhouse warming. *Journal of Climate*, *33*, 675–690. https://doi.org/10.1175/JCLI-D-19-0376.1

Wang, G., Cai, W., Yang, K., Santoso, A., & Yamagata, T. (2020b). A unique feature of the 2019 extreme positive Indian Ocean Dipole event. *Geophysical Research Letters*, *47*, e2020GL088615. https://doi.org/10.1029/2020GL088615

Wang, X., & Wang, C. (2014). Different impacts of various El Niño events on the Indian Ocean Dipole. *Climate Dynamics*, *42*(3), 991–1005. https://doi.org/10.1007/s00382-013-1711-2

Webster, P. J., Moore, A. M., Loschnigg, J. P., & Leben, R. R. (1999). Coupled ocean–atmosphere dynamics in the Indian Ocean during 1997–98. *Nature*, *401*(6751), 356–360. https://doi.org/10.1038/43848

Xie, S.-P., Annamalai, H., Schott, F. A., & McCreary, J. P. (2002). Structure and mechanisms of South Indian Ocean climate variability. *Journal of Climate*, *15*(8), 864–878. https://doi.org/10.1175/1520-0442(2002)015<0864:SAMOSI>2.0.CO;2

Yang, K., Cai, W., Huang, G., Wang, G., Ng, B., & Li, S. (2020). Oceanic processes in ocean temperature products key to a realistic presentation of positive Indian Ocean Dipole nonlinearity. *Geophysical Research Letters*, *47*(16), e2020GL089396. https://agupubs.onlinelibrary.wiley.com/doi/abs/10.1029/2020GL089396

Yang, Y., Xie, S.-P., Wu, L., Kosaka, Y., Lau, N.-C., & Vecchi, G. A. (2015). Seasonality and predictability of the Indian Ocean Dipole Mode: ENSO forcing and internal variability. *Journal of Climate*, *28*(20), 8021–8036. https://doi.org/10.1175/JCLI-D-15-0078.1

Zhang, W., Wang, Y., Jin, F.-F., Stuecker, M. F., & Turner, A. G. (2015). Impact of different El Niño types on the El Niño/IOD relationship. *Geophysical Research Letters*, *42*(20), 8570–8576. https://agupubs.onlinelibrary.wiley.com/doi/abs/10.1002/2015GL065703

Zhao, S., Jin, F.-F., & Stuecker, M. F. (2019). Improved predictability of the Indian Ocean Dipole using seasonally modulated ENSO forcing forecasts. *Geophysical Research Letters*, *46*(16), 9980–9990. https://doi.org/10.1029/2019GL084196